PHYSICAL REVIEW B **105**, 045405 (2022)

Electron trapping in twisted light driven graphene quantum dots

Adrian Pena

National Institute of Materials Physics, Atomiştilor 405A, 077125 Măgurele –Ilfov, Romania
and Faculty of Physics, University of Bucharest, Atomiştilor 405, 077125 Măgurele – Ilfov, Romania

(Received 6 August 2021; revised 9 September 2021; accepted 3 January 2022; published 10 January 2022)

In this paper, we present a theoretical perspective concerning the scattering of electrons on a twisted light (TL) driven graphene quantum dot (GQD). Relatively recently discovered, TL is a novel type of electromagnetic field which carries a finite orbital angular momentum oriented on the propagation direction, besides its spin. This striking property of TL is due to its spatial structure. It is well known that the localization of electrons in a GQD is forbidden by the Klein tunneling, an effect that manifests by the perfect transmission of electrons through a potential barrier, regardless of its magnitude. Here we demonstrate that, for a suitable choice of the scattering regimes, there emerge scattering resonances characterized by trapping states of the incident electron inside the GQD for finite periods of time. The most interesting result is the prediction regarding the possibility to control the trapping times using a TL irradiation. Also, we mention that the investigation was performed for a frequency of the TL within the infrared spectrum.

DOI: 10.1103/PhysRevB.105.045405

I. INTRODUCTION

Interaction of graphene with external fields such as electromagnetic [1–7], magnetic [8–12], or combinations of different types of fields [13–15] has been the subject of some wide studies concluding very promising results with potential applications in the nanoscale technology development. Moreover, much attention was payed to the problem of transport through different devices based on graphene such as field effect transistors, phototransistors, light detection devices, graphene based optoelectronic devices, and so on [16–19].

In the recent years, twisted light (TL), a novel type of spatially structured electromagnetic field, was the subject of a new branch of Optics, as well as its interaction with atoms [20–22] and also with graphene [23]. The peculiar characteristic of TL consists in its intrinsic property to carry a nonzero orbital angular momentum, determined by its spatial distribution and being independent of the polarization. During the propagation of TL, the wavefront resembles a corkscrewlike pattern and the wave vector rotates around the propagation direction describing a cone with a well defined opening angle. From a corpuscular point of view, the photons propagate rotating around the center of the beam and this motion specific to a nonzero orbital angular momentum gives the name *twisted light*. In the center of the beam one sees a singularity, called *optical vortex*, where the intensity of the optical field vanishes and, as the radial coordinate increases, a sequence of zeros and local maxima occurs.

Due to the peculiar properties of low energy electrons in graphene, of behaving like massless Dirac fermions [24,25], the localization of an electron in a graphene quantum dot (GQD) is forbidden by the Klein tunneling. This striking effect specific to graphene is the solid-state counterpart of the relativistic Klein paradox which manifests by perfect transmission of relativistic energies electrons through an electrostatic potential barrier, regardless of its magnitude.

Even though, it was reported that in circular graphene *p*-*n* junctions defined GQDs [26] or in GQDs produced by substrate engineering [27] a weakly trapping of electrons may be achieved. As well, an other method to enhance the trapping time of electrons in GQDs was by applying an external magnetic field [28,29]. Because it is not a really bound state (e.g., as in an atom), in the case of a trapped electron, its state is called *quasibound state* and the localization is substituted by *quasilocalization*.

Besides the interest shown in solid-state graphene based devices, the unique properties of graphene discussed above create a perfect playground to study also the fundamental problem of field-matter interaction. We can take advantage of a very elegant and somehow straightforward method to study the problem in question, namely manipulate the Dirac equation in order to describe the way the Dirac fermions dynamics is affected by the TL driving.

In this paper, we are proposing an analytical model for the interaction of Dirac fermions in a GQD with TL and, based on this model, we investigate the scattering problem of electrons on TL driven GQDs. To this end, we make use of the Floquet theory in order to deal with an easier, associated stationary problem. Furthermore, we perform numerical calculations which reveal important results, related to the trapping of electrons inside the GQDs. The investigation is largely based on the quasilocalization of the electrons and the lifetime of their quasibound states (trapping time).

The present paper is organized as follows. In Sec. II, we elaborate a model for interaction of Dirac fermions in graphene with TL, namely, we present a perturbation method for solving the Dirac equation in the case of mesoscopic systems. In Sec. III, we make use of the solutions derived in the

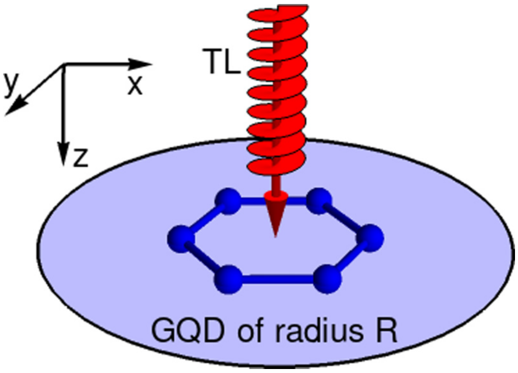

FIG. 1. Schematic description of the studied system. The GQD is placed on the horizontal xy plane and the TL is propagating on z axis, at normal incidence on the GQD.

previous section in order to model the scattering of electrons on a TL driven GQD and present the main numerical results. Finally, we summarize the results and discuss their importance from both the fundamental and applicability points of view.

II. ANALYTICAL MODEL FOR INTERACTION OF DIRAC FERMIONS IN A GQD WITH TL

The energy dispersion in graphene, in the vicinity of high symmetry Dirac K points in the Brillouin zone, is known to be linear with the small displacement wave vector $\boldsymbol{\kappa}$ around the wave vector $\mathbf{K}$ corresponding to each K point, $E_k = \pm\hbar v_F|\boldsymbol{\kappa} - \mathbf{K}|$. Here, $\hbar$ is the reduced Planck constant and $v_F \approx c/300$ is the Fermi velocity with c the speed of light in vacuum. Consequently, in this low-excitations regime around K points, the charged particles in graphene behave like massless Dirac fermions [30], moving freely with Fermi velocity v_F.

In this section, we present a model which describes the interaction of Dirac fermions in a circular GQD with TL, considering single particle states and assuming no intervalley scattering. We consider a GQD lying in xy plane supposed to a TL beam irradiation propagating on z direction, at normal incidence on the dot. The studied system is displayed in Fig. 1.

In order to describe the state of these quasiparticles supposed to a TL beam driving, one can formulate a time-dependent Dirac equation, considering minimal coupling of electromagnetic radiation (real spin degree of freedom neglected):

$$H(\boldsymbol{r},t)\psi(\mathbf{r},t) = i\hbar\partial_t\psi(\mathbf{r},t); \tag{1}$$

$$H(\boldsymbol{r},t) = H_0(\boldsymbol{r},t) - ev_F\boldsymbol{\sigma}\cdot\mathcal{A}(\boldsymbol{r},t). \tag{2}$$

Given the geometry of the studied system, here and in the following, we adopt a polar coordinates reference system with $\boldsymbol{r} = (r,\varphi)$ and set the origin in the center of the GQD. Here, $H(\mathbf{r},t)$ [Eq. (2)] is the full Hamiltonian which describes the dynamics of Dirac fermions in graphene under TL irradiation. The first term in Eq. (2) $H_0(\boldsymbol{r},t) = -iv_F\hbar\boldsymbol{\sigma}\cdot\nabla$, with $\nabla \equiv (\partial_r, \frac{1}{r}\partial_\varphi)$, is the free Hamiltonian for a massless Dirac fermion and the second term, which contains the vector potential of TL [$\mathcal{A}(\boldsymbol{r},t)$], introduces the interaction in our problem.

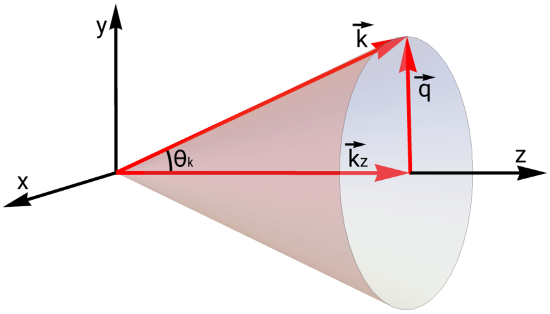

FIG. 2. The geometry of TL propagation. During the propagation, the wave vector $\mathbf{k} = \mathbf{q} + \mathbf{k_z}$ is rotating about the propagation direction (z axis), describing a cone with a well defined opening angle θ_k. The transversal wave vector is denoted by $\mathbf{q}$ and, respectively, the longitudinal wave vector by $\boldsymbol{k}_z$.

Moreover, in Eq. (2), $\boldsymbol{\sigma} = (\sigma_r, \sigma_\varphi)$ is the Pauli vector whose components are the Pauli matrices, which in polar coordinates read [31]

$$\sigma_r = \begin{pmatrix} 0 & e^{-i\varphi} \\ e^{i\varphi} & 0 \end{pmatrix}; \quad \sigma_\varphi = \begin{pmatrix} 0 & -ie^{-i\varphi} \\ ie^{i\varphi} & 0 \end{pmatrix}. \tag{3}$$

There are many possibilities to introduce the interaction with TL and in the present work we choose the Bessel representation, more detailed introduced in Refs. [21,22]. Let us shortly discuss the geometry of TL propagation, see Fig. 2. We choose z axis as the propagation direction. As the wave front goes by, the wave vector $\mathbf{k}$ rotates around the propagation direction defining a cone with a well defined opening angle $\theta_k = \arctan(q/k_z)$, where q is the magnitude of the transversal wave vector $\mathbf{q}$ and k_z is the magnitude of the longitudinal wave vector $\boldsymbol{k}_z$.

The vector potential of TL reads with the following formula [23,32]:

$$\boldsymbol{A}(\boldsymbol{r},t) = A_0\left(J_m(qr)e^{im\varphi}\boldsymbol{\epsilon}_\Lambda - \Lambda i\frac{q}{k_z}J_{m+\Lambda}(qr)e^{i(m+\Lambda)\varphi}\hat{\boldsymbol{z}}\right) \times e^{i(k_z z - \omega t)}. \tag{4}$$

Here, A_0 is a real constant amplitude, m is the topological charge, ω is the frequency of the electromagnetic field and $\boldsymbol{\epsilon}_\Lambda = \hat{\boldsymbol{x}} + \Lambda i\hat{\boldsymbol{y}}$ is the polarization vector in xy plane with $\Lambda = \pm 1$ the helicity quantum number. Given the 2D geometry of the studied system, the longitudinal component of the vector potential does not participate to the interaction and, of course, without losing the generality, the "physical" vector potential introduced in Eq. (2) reads with the following expression:

$$\begin{aligned}\mathcal{A}(\boldsymbol{r},t) &= \Re\{\boldsymbol{A}(\boldsymbol{r},t)\}|_{z=0} \\ &= A_0 J_m(qr)[\cos(m\varphi - \omega t)\hat{\boldsymbol{x}} + \Lambda\sin(m\varphi - \omega t)\hat{\boldsymbol{y}}].\end{aligned} \tag{5}$$

Since the Hamiltonian (2) is periodic in time with the period $T = 2\pi/\omega$, in order to model the interaction, we employ the Floquet theorem which guarantees that the eigenvalue equation associated to a time-periodic Hamiltonian [$H(\boldsymbol{r},t) = H(\boldsymbol{r},t+T)$] admits particular solutions which have the following structure [33,34]:

$$\psi(\boldsymbol{r}) = e^{-iWt/\hbar}\phi(\boldsymbol{r},t). \tag{6}$$

The states described by Floquet solutions (6) are called *Floquet states* and W is called *quasienergy*, which is defined up to an integer multiple of $\hbar\omega$, $\widetilde{W} = W + N\hbar\omega$. Note that $\phi(\boldsymbol{r}, t)$ has the same periodic feature as the Hamiltonian, $\phi(\boldsymbol{r}, t) = \phi(\boldsymbol{r}, t + T)$.

By introducin g the Floquet solution (6) into the time-dependent Dirac Eq. (1), we obtain the following eigenvalue equation for the quasienergy:

$$H_F(\boldsymbol{r}, t)\psi(\boldsymbol{r}, t) = W\psi(\boldsymbol{r}, t); \tag{7}$$

$$H_F(\boldsymbol{r}, t) = H(\boldsymbol{r}, t) - i\hbar\partial_t. \tag{8}$$

Here, $H_F(\boldsymbol{r}, t)$ is called *Floquet Hamiltonian*. The problem we address now is the eigenvalue equation associated to the Floquet Hamiltonian (8) and it is still time-dependent. In what follows, we present the derivation of an associated stationary problem in the approximation of an effective Hamiltonian.

Taking into account the time-periodicity of both the Hamiltonian (2) and the Floquet solution (6), one can express them in terms of Fourier series:

$$H(\boldsymbol{r}, t) = \sum_{n=-\infty}^{\infty} e^{-in\omega t} H_n(\boldsymbol{r}); \tag{9}$$

$$\phi(\boldsymbol{r}, t) = \sum_{n=-\infty}^{\infty} e^{-in\omega t} \phi_n(\boldsymbol{r}). \tag{10}$$

The following corresponding inverse transformations:

$$H_n(\boldsymbol{r}) = \frac{1}{T}\int_0^T e^{in\omega t} H(\boldsymbol{r}, t)dt; \tag{11}$$

$$\phi_n(\boldsymbol{r}) = \frac{1}{T}\int_0^T e^{in\omega t} \phi(\boldsymbol{r}, t)dt, \tag{12}$$

may be performed using the orthonormalization relation of Fourier functions, $\frac{1}{T}\int_0^T e^{i(n-m)\omega t}dt = \delta_{nm}$, where δ_{nm} is the Kronecker symbol.

Manipulating Eqs. (7)–(12), we end with the following infinite system of coupled equations for the Fourier components $\phi_n(\mathbf{r})$:

$$\left(\sum_{m=-\infty}^{\infty} H_{m-n} + m\hbar\omega\delta_{mn}\right)\phi_m(\mathbf{r}) = W\phi_n(\mathbf{r}); \quad n = -\infty, \dots, 1, 0, 1, \dots, \infty, \tag{13}$$

called *Floquet system of equations*.

Analyzing the Floquet system of equations one should observe that the energy spectrum consists in an infinite sequence of copies of $H_0(\mathbf{r})$ spectrum (Floquet bands), separated by an amount of energy equal to $\hbar\omega$. The Floquet bands are mixed by the terms H_{m-n} with $m \neq n$. Depending on the magnitude of $\hbar\omega$ with respect to the bandwidth of the eigenvalues of $H_0(\mathbf{r})$, which in our case corresponds to the typical energies around Dirac points, we can establish how much the mixing of two adjacent Floquet bands affects the problem. Therefore the problem of Floquet system of equations should be firstly analyzed in terms of specific energy scales. In what follows, we drop the notation $\mathbf{r}$ and introduce the explicit notation (r, φ).

In the case of a nonresonant regime [35], characterized by high energy $\hbar\omega$, the Floquet system of equations can be truncated and the problem reduces to the following eigenvalue equation [36,37] :

$$(H_{\text{eff}} - W)\phi_\kappa(r, \varphi) = 0; \tag{14}$$

$$H_F^{\text{eff}} = H_0 + \frac{1}{\hbar\omega}[H_{-1}, H_1]. \tag{15}$$

Here, H_F^{eff} is the first nontrivial order effective Floquet Hamiltonian. The first term in Eq. (15) is the time averaged Hamiltonian over a cycle of oscillation of the TL electromagnetic field, which corresponds to the zero-photon states. The second term expresses the second order of perturbation, due to virtual processes of absorption/emission of a photon [38].

Taking into account the form of the "physical" vector potential (5) and the inverse Fourier transformation (11), we compute

$$H_{-1} = -\frac{ev_F A_0}{2} J_m(qr)e^{-im\varphi}(\sigma_x + i\Lambda\sigma_y); \tag{16}$$

$$H_1 = -\frac{ev_F A_0}{2} J_m(qr)e^{im\varphi}(\sigma_x - i\Lambda\sigma_y). \tag{17}$$

Finally, the commutator involved in the expression of the effective Hamiltonian (15) reads

$$[H_{-1}, H_1] = \Lambda(ev_F A_0)^2 J_m^2(qr)\sigma_z. \tag{18}$$

Gathering all the results above we derive the following equation for $\phi_\kappa(r, \varphi)$:

$$(-i\boldsymbol{\sigma}\cdot\boldsymbol{\nabla} - \kappa + \Lambda\lambda^{-1}\Gamma(r)\sigma_z)\phi_\kappa(r, \varphi) = 0, \tag{19}$$

where we have introduced the following notations:

$$\kappa = W/v_F\hbar; \tag{20}$$

$$\lambda^{-1} = v_F(eA_0)^2/\hbar^2\omega; \tag{21}$$

$$\Gamma(r) = J_m^2(qr). \tag{22}$$

Here κ stands for the associated wave number of the Dirac fermion in the TL driven GQD. Eq. (19) is a first order matrix differential equation for the unknown spinor $\phi_\kappa(r, \varphi) = (\phi_\kappa^A, \phi_\kappa^B)^T$ and can be decomposed in a system of two coupled, second-order differential equations for the unknown functions ϕ_κ^A and ϕ_κ^B. Even though, the system of differential equations can not be solved exactly.

Equation (19) seems similar to free Dirac equation upon the term proportional to λ^{-1}, thus at the first glance, one could be tempted to apply a perturbation method to solve the equation for the case of $\lambda^{-1} \ll \kappa$. Leaving behind this condition which is very coercive and unnecessary, we anticipate that even for high values of λ^{-1}, its corresponding term acts like a perturbation, introducing only a small correction in the solution $\phi_\kappa(r, \varphi)$ with respect to the solution of free Dirac equation, in the case of a suitable choice of the parameters (i.e., Dirac fermion wave number, radius of the dot, amplitude of the vector potential, frequency, and so on). Therefore, making this assumption, we seek the solution in the following form:

$$\phi_\kappa(r, \varphi) \approx \phi_0(r, \varphi) + \lambda^{-1}\zeta(r, \varphi). \tag{23}$$

Here we have introduced the spinor

$$\phi_0(r,\varphi)=\begin{pmatrix} J_l(\kappa r)e^{il\varphi}\\ \alpha iJ_{l+1}(\kappa r)e^{i(l+1)\varphi}\end{pmatrix}, \tag{24}$$

which satisfies the unperturbed (free) Dirac equation $(-i\sigma\cdot\nabla-\alpha|\kappa|)\phi_0(r,\varphi)=0$ [39]. Here, $\alpha=\pm1$, called *band index*, stands for positive energy (conduction band, CB) and, respectively, for negative energy (valence band, VB) states, $E=\alpha v_F\hbar\kappa$. In what follows, our aim is to pursue the derivation of the correction spinor $\zeta(r,\varphi)=(\zeta_A,\zeta_B)^T$.

Substituting the free Dirac spinor (24) into the full solution (23) and plugging it into Eq. (19) we find the following equation for the sought spinor $\zeta(r,\varphi)$, for the first order of perturbation:

$$(-i\sigma\cdot\nabla-\alpha|\kappa|)\zeta(r,\varphi)+\Lambda\Gamma(r)\sigma_z\phi_0(r,\varphi)=0. \tag{25}$$

The special form of the above equation suggests to make the following ansatz:

$$\zeta(r,\varphi)=S(r,\varphi)\chi(r). \tag{26}$$

Here, $\chi(r)=(\chi_A(r),\chi_B(r))^T$ is a spinor whose components depend only on the radial coordinate and the newly introduced factor $S(r,\varphi)$ is the fundamental matrix of the system of coupled differential equations $(-i\sigma\cdot\nabla-\alpha|\kappa|)(s_1(r,\varphi),s_2(r,\varphi))^T=0$:

$$S(r,\varphi)=\begin{pmatrix} J_l(\kappa r)e^{il\varphi} & Y_l(\kappa r)e^{il\varphi}\\ \alpha iJ_{l+1}(\kappa r)e^{i(l+1)\varphi} & \alpha iY_{l+1}(\kappa r)e^{i(l+1)\varphi}\end{pmatrix}. \tag{27}$$

Here, $Y_l(x)$ is the Bessel function of the second kind of l th order and all possible constant factors were chosen by convention equal to unity. Note that each column contains linearly independent terms, thus the matrix is nonsingular and consequently we are assured that the inverse matrix exists:

$$S^{-1}(r,\varphi)=\frac{\pi kr}{2}\begin{pmatrix} -Y_{l+1}(\kappa r)e^{-il\varphi} & -\alpha iY_l(\kappa r)e^{-i(l+1)\varphi}\\ J_{l+1}(\kappa r)e^{-il\varphi} & \alpha iJ_l(\kappa r)e^{-i(l+1)\varphi}\end{pmatrix}. \tag{28}$$

If we introduce ansatz (26) into Eq. (25), the differential equations which compose the system are still coupled, but we can decouple them by factorizing Eq. (25) at the left-hand side with $S^{-1}(r,\varphi)\sigma_r$, and performing the calculations we end with the following differential equations for $\chi_A(r)$ and $\chi_B(r)$, respectively:

$$\partial_r\chi_A(r)+\frac{\Lambda\pi\kappa r}{2}[\alpha Y_l(\kappa r)J_l(\kappa r)-Y_{l+1}(\kappa r)J_{l+1}(\kappa r)]\Gamma(r)=0; \tag{29}$$

$$\partial_r\chi_B(r)-\frac{\Lambda\pi\kappa r}{2}\left[\alpha J_l^2(\kappa r)-J_{l+1}^2(\kappa r)\right]\Gamma(r)=0. \tag{30}$$

For $\Gamma(r)$ as it was defined in Eq. (22), Eqs. (29) and (30) can not be integrated analytically, but one more trick can be employed. If we are dealing with mesoscopic systems where the radius of the GQD is of order of 10^2 nm and the typical frequencies of the TL are $\omega<10^{15}\ \mathrm{s}^{-1}$, then we can make use of the following approximation for Bessel functions for small arguments, $J_m(x)\approx(x/2)^m/\Gamma(m+1)$, thus $\Gamma(r)\approx 1/\Gamma^2(m+1)(qr/2)^{2m}$. With this assumption, using the following identities [40,41]:

$$J_l(x)Y_l(x)=-\frac{1}{\sqrt{\pi}}G^{20}_{13}\left(x^2\middle|\begin{matrix}\frac{1}{2}\\ 0,\,l,\,-l\end{matrix}\right); \tag{31}$$

$$J_l^2(x)=\frac{x^{2l}}{2^{2l}\Gamma^2(l+1)}\,{}_1F_2\left(-x^2\middle|\begin{matrix}l+\frac{1}{2}\\ l+1,\,2l+1\end{matrix}\right), \tag{32}$$

where the notation $G^{pq}_{mn}(x)$ refers to the Meijer G function and, respectively, ${}_pF_q(x)$ to generalized hypergeometric function, Eqs. (29) and (30) can be forwardly integrated using the integration relations provided by Refs. [42,43]. Thus we end with the following solutions:

$$\chi_A(r)=\frac{\Lambda\sqrt{\pi}r(\kappa r)(qr)^{2m}}{2^{2(m+1)}\Gamma^2(m+1)}\left[\alpha G^{2,1}_{2,4}\left(\kappa^2r^2\middle|\begin{matrix}-m,\,\frac{1}{2}\\ 0,\,l,\,-l,\,-m-1\end{matrix}\right)-G^{2,1}_{2,4}\left(\kappa^2r^2\middle|\begin{matrix}-m,\,\frac{1}{2}\\ 0,\,l+1,\,-l-1,\,-m-1\end{matrix}\right)\right]; \tag{33}$$

$$\chi_B(r)=\frac{\Lambda\pi r(qr)^{2m}(\kappa r)^{2l+1}}{2^{2(l+m+2)}\Gamma^2(m+1)}\left[\alpha\frac{4\,{}_2F_3\left(-\kappa^2r^2\middle|\begin{matrix}l+m+1,\,l+\frac{1}{2}\\ l+m+2,\,l+1,\,2l+1\end{matrix}\right)}{(l+m+1)\Gamma^2(l+1)}-\frac{(\kappa r)^2\,{}_2F_3\left(-\kappa^2r^2\middle|\begin{matrix}l+m+2,\,l+\frac{3}{2}\\ l+m+3,\,l+2,\,2l+3\end{matrix}\right)}{(l+m+2)\Gamma^2(l+2)}\right]. \tag{34}$$

To summarize, the perturbatively derived spinor solution of the stationary Dirac Eq. (19), which defines the state of a Dirac fermion in a TL driven GQD, reads

$$\phi_\kappa(r,\varphi)=\begin{pmatrix}\phi^A_\kappa(r)e^{il\varphi}\\ \alpha i\phi^B_\kappa(r)e^{i(l+1)\varphi}\end{pmatrix}; \tag{35}$$

$$\phi^A_\kappa(r)=J_l(\kappa r)+\lambda^{-1}[J_l(\kappa r)\chi_A(r)+Y_l(\kappa r)\chi_B(r)]; \tag{36}$$

$$\phi^B_\kappa(r)=J_{l+1}(\kappa r)+\lambda^{-1}[J_{l+1}(\kappa r)\chi_A(r)+Y_{l+1}(\kappa r)\chi_B(r)]. \tag{37}$$

Note that the spinor (35) is an eigenfunction of the total angular momentum operator $J_z=L_z+S_z$ for the eigenvalue $l+1/2$. Here, $L_z=-i\hbar\partial_\varphi$ is the orbital angular momentum operator and, respectively, $S_z=\hbar/2\sigma_z$ is the spin operator where

$$\sigma_z = \begin{pmatrix} 1 & 0 \\ 0 & -1 \end{pmatrix}. \tag{38}$$

Therefore the spinor (35) describes a state of well defined orbital angular momentum, as a consequence of the azimuthal symmetry of the effective Floquet Hamiltonian (15).

III. SCATTERING ANALYSIS OF ELECTRONS ON A TL DRIVEN GQD

A. Theory

In this section, we investigate the elastic scattering process of electrons on a circular TL driven GQD. Let us firstly describe the physical process and introduce the main equations. We keep the reference system centered on the GQD. The incident electron travels freely towards the GQD on x direction with energy $E = v_F \hbar k$ with k the associated wave number, therefore its corresponding wave function is a plane wave:

$$\psi_k^i(r,\varphi) = \frac{1}{\sqrt{2}} e^{ikr\cos\varphi} \begin{pmatrix} 1 \\ 1 \end{pmatrix} = \frac{1}{\sqrt{2}} \sum_{n=-\infty}^{\infty} i^n \begin{pmatrix} J_n(kr) e^{in\varphi} \\ iJ_{n+1}(kr) e^{i(n+1)\varphi} \end{pmatrix}. \tag{39}$$

Note that the wave function of the incident electron was decomposed in an infinite sum of well defined orbital angular momentum states making use of Jacobi-Anger expansion $e^{iz\cos\varphi} = \sum_{n=-\infty}^{\infty} i^n J_n(z) e^{in\varphi}$. The transmitted electron inside the GQD is represented by a wave function based on the solutions of Dirac equation derived in the previous section:

$$\psi_\kappa^t(r,\varphi) = \sum_{n=-\infty}^{\infty} c_n^t \begin{pmatrix} \phi_\kappa^A e^{in\varphi} \\ \alpha i \phi_\kappa^B e^{i(n+1)\varphi} \end{pmatrix}. \tag{40}$$

The reflected particle can be described in terms of partial waves as follows:

$$\psi_k^r(r,\varphi) = \frac{1}{\sqrt{2}} \sum_{n=-\infty}^{\infty} i^n c_n^r \begin{pmatrix} H_n(kr) e^{in\varphi} \\ iH_{n+1}(kr) e^{i(n+1)\varphi} \end{pmatrix}. \tag{41}$$

Here, H_n refers to nth-order Hankel functions of the first kind, which are also solutions of free Dirac equation for well defined orbital angular momentum and, moreover, represent outgoing waves satisfying the infinite boundary condition requested by the physics of the scattering process [44], $H_n(z) \propto \sqrt{\frac{2}{\pi z}} e^{i(z - \frac{l\pi}{2} - \frac{\pi}{4})}$ for $z \gg 1$. The process is schematically described in Fig. 3. The reflection and transmission coefficients, c_n^r and c_n^t, are to be derived by imposing the appropriate boundary conditions for the wave functions. For instance, in Ref. [45], the different scattering mechanisms are presented for the case without light irradiation. Since at limit for $A_0 \to 0$, Eq. (35) reduces to the free spinor and a finite A_0 (irradiation switched on) modifies perturbatively the wave functions (36) and (37), we are intended to impose the following boundary condition, suggested in Ref. [45]:

$$\psi_k^i(R,\varphi) + \psi_k^r(R,\varphi) = \psi_\kappa^t(R,\varphi). \tag{42}$$

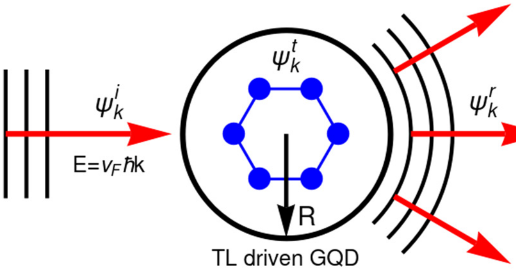

FIG. 3. Schematic description of the scattering process. The incident electron described by the wave function ψ_k^i travels towards the GQD of radius R with a well defined energy, $E = v_F \hbar k$. After the interaction with the TL driven GQD, the electron either is reflected in the outer side of the dot (obeying the energy conservation laws specific to an elastic scattering) and its state is described by ψ_k^r, or it resides inside the dot and its state is described by ψ_κ^t.

Performing the calculations, we end with the following scattering coefficients:

$$c_n^t = \frac{\sqrt{2} e^{i\frac{(n+1)\pi}{2}}}{\pi kr\left[H_n(kr)\phi_\kappa^B(r) - H_{n+1}(kr)\phi_\kappa^A(r)\right]}; \tag{43}$$

$$c_n^r = \frac{J_n(kr)\phi_\kappa^B(r) - J_{n+1}(kr)\phi_\kappa^A(r)}{H_{n+1}(kr)\phi_\kappa^A(r) - H_n(kr)\phi_\kappa^B(r)}. \tag{44}$$

In what follows, we introduce the definitions for the most important quantities which characterize the scattering process. The probability density is given by $\rho = \psi^\dagger \psi$ and, respectively, the current by $\mathbf{j} = \psi^\dagger \boldsymbol{\sigma} \psi$. Here $\psi = \psi_\kappa^t(r,\varphi)$ corresponds to transmitted electron inside the GQD and, respectively, $\psi = \psi_k^i(r,\varphi) + \psi_k^r(r,\varphi)$ to an electron originating from outside GQD region. For the case of only the reflected electron, we substitute $\psi = \psi_k^r(r,\varphi)$. Based on the property of Bessel functions $Z_{-n}(z) = (-1)^n Z_n(z)$ with $Z = J$ or Y, we find that $\chi_{A(B)}$ are invariant under the change of sign of l [see Eqs. (29) and (30)] and $c_{-l}^{t(r)} = c_{l-1}^{t(r)}$. This property allows us to rearrange the terms in Eqs. (40) and (41) and use the following expressions for the wave functions:

$$\psi_\kappa^t(r,\varphi) = \frac{1}{\sqrt{2}} \sum_{n=0}^{\infty} i^n c_n^t \left[\phi_\kappa^A \begin{pmatrix} e^{in\varphi} \\ e^{-in\varphi} \end{pmatrix} + \alpha i \phi_\kappa^B \begin{pmatrix} e^{-i(n+1)\varphi} \\ e^{i(n+1)\varphi} \end{pmatrix}\right]; \tag{45}$$

$$\psi_k^r(r,\varphi) = \frac{1}{\sqrt{2}} \sum_{n=0}^{\infty} i^n c_n^r \left[H_n(kr) \begin{pmatrix} e^{in\varphi} \\ e^{-in\varphi} \end{pmatrix} + iH_{n+1}(kr) \begin{pmatrix} e^{-i(n+1)\varphi} \\ e^{i(n+1)\varphi} \end{pmatrix}\right]. \tag{46}$$

Using the wave function (46) and the asymptotic behavior of Hankel functions of the first kind recalled above, the radial component of the far field reflected current is given by

$$j_{\text{rad}}(r,\varphi) = \frac{4}{\pi kr} \sum_{n=0}^{\infty} \left|c_n^r\right|^2 [\cos((2n+1)\varphi + 1)] + \frac{8}{\pi kr} \sum_{n'<n} \text{Re}\left(c_n^r c_{n'}^r\right) [\cos((n+n'+1)\varphi) + \cos((n-n')\varphi)]. \tag{47}$$

Taking into account that the scattering analysis implies also the investigation of the way that the scattering effects are affected by the radius of the GQD, we introduce the scattering efficiency which is defined as the scattering cross section divided by the geometric cross section [46,47]:

$$Q = \frac{4}{kR}\sum_{n=0}^{\infty}\left|c_n^r\right|^2. \tag{48}$$

B. Main numerical results

In this section, we present the main numerical results based on the theory shortly introduced in the previous section and respecting the limitations we have discussed about in Sec. II. For the characterization of the process, we will describe the behavior of scattering efficiency (Q), probability density (ρ) and current ($\mathbf{j}$) with respect to the modification of the GQD radius (R) and the amplitude of the vector potential (A_0). Since TL exhibits a nonuniform spatial distribution of its intensity, the scattering analysis may be performed with respect to A_0, which is a constant or otherwise, in order to keep the investigation consistent and use conventional units, we introduce $P_{\rm GQD}$, a quantity which represents the averaged total power of TL which irradiates the GQD over a period of oscillation. The definition and derivation are presented in Appendix. The newly introduced quantity is related to A_0 by

$$P_{\rm GQD}(\rm mW) = \beta A_0^2(\mu V\,s\,m^{-1}). \tag{49}$$

We notice that in the following we refer to $P_{\rm GQD}$ simply as "TL power."

Preliminary we mention that the scattering process is more conveniently analyzed in terms of *scattering modes* which are indexed by n ranging from 0 to ∞ [see Eqs. (45)–(48)]. We consider in our analysis that only normal scattering modes are excited. In the whole work, we limit ourselves to the case of topological charge $m = 1$, angular frequency $\omega = 10^{14}$ s^{-1}, and opening angle $\theta_k = 30^\circ$.

Taking into account that TL is a special type of electromagnetic field which possess both spin and orbital angular momentum we concentrate at the very beginning on this extraordinary feature. Let us firstly investigate the scattering efficiency as a function of R and A_0 for the scattering modes $n = 0$ and $n = 1$, which are the only excited scattering modes. This first investigation serves us as a starting point for a further analysis using values of interest for R and A_0. The studied system consists in an incident electron that scatters on a TL driven GQD on which an electrostatic bias $V > 0$ is applied [48]. The band structure of the system is displayed in Fig. 4. Firstly, let us briefly describe the process. The incident electron with energy $E = v_F\hbar k$, lies in the CB (at Fermi level, in the upper Dirac cone) until it enters the dot. Once it penetrates the barrier, in the biased region where the applied potential shifts the Fermi level towards lower values, its energy lies either in CB ($\alpha = +1$) or in VB ($\alpha = -1$), depending on the strength of the potential. In this case, its corresponding wave number will be $\kappa = |E - V|/(v_F\hbar)$.

In Fig. 5(a), we present the results for the case of $\Lambda = 1$ (positive helicity), in which case the spin and orbital angular momentum of TL have the same orientation. The energy of the incident electron was chosen $E = 0.5$ meV. In Fig. 5(b), we considered $\Lambda = -1$ (negative helicity) for the same energy of the incident electron as in panel (a). In this case, the spin and orbital angular momentum of the TL are oriented in opposite directions. Since the scattering efficiency is a measure of the interaction strength between the incident electron and the dot, it can be observed that for both types of helicity, the TL driving is mandatory for giving rise to relevant scattering phenomena. As revealed in panels (a) and (b), there is imposed a value of $A_0 \approx 1\ \mu$Vs/m below which the interaction is very weak, basically absent. For higher values of A_0 the scattering effect is governed by the helicity of the TL, as we will describe in what follows. For the case of $\Lambda = 1$, the scattering efficiency is rising monotonously with A_0 for a fixed R and reaches values much lower than for negative helicity. For the case of $\Lambda = -1$, the important values of scattering efficiency lie on a strip of values for A_0 and R. This behavior is associated with so called *scattering resonances* which generally are characterized by trapping phenomena of the incident electron inside the dot [49,50]. As well, each resonance is assigned to a given scattering mode. In our studied case, the resonance which occur at lower values of A_0 is due to the excitation of $n = 0$ scattering mode, while the second which exhibits higher values of scattering efficiency and a much narrower strip is due to the excitation of $n = 1$ mode, as indicated on the plot.

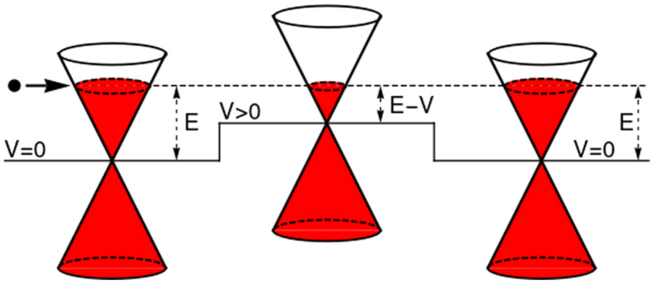

FIG. 4. The band structure corresponding to biased ($V > 0$)/nonbiased ($V = 0$) regions. The GQD is defined in the biased region (the center Dirac cones). The incident electron with energy $E = v_F\hbar k$ enters the CB in nonbiased region. Inside the dot the applied electrostatic potential reduces the Fermi level and the energy of the electron is $E = v_F\hbar\kappa$ where $\kappa = |E - V|/(v_F\hbar)$ is the associated wave number. Outside the dot the potential is $V = 0$ then, by virtue of conservation laws, the energy of the electron is $E = v_F\hbar k$.

In Fig. 5(c), the scattering efficiency is plotted as a function of the TL power, for $R = 220$ (red curve) and 280 nm (blue curve), as indicated by white vertical dashed lines in panel (b). In these two cases, the values of $P_{\rm QGD}$ defined in Eq. (49) were evaluated using $\beta = 0.68$ and 1.8 for $R = 220$ and 280 nm, respectively, as computed in Appendix. For each curve, the corresponding axis of $P_{\rm GQD}$ values is indicated by an arrow of specific color.

In the case of $R = 220$ nm, the only excited scattering mode is $n = 0$. The line shape shows a very asymmetric specific Lorentz profile with the peak centered on $P_{\rm GQD} = 4.95$ mW (see label "2"). This asymmetry of the profile occurs due to the Fano resonance phenomenon, which consists in the interference of a resonantly excited scattering mode (n = 0 in our case) with the slowly varying background [51]. For $R = 280$ nm besides $n = 0$, there arises also $n = 1$ scattering

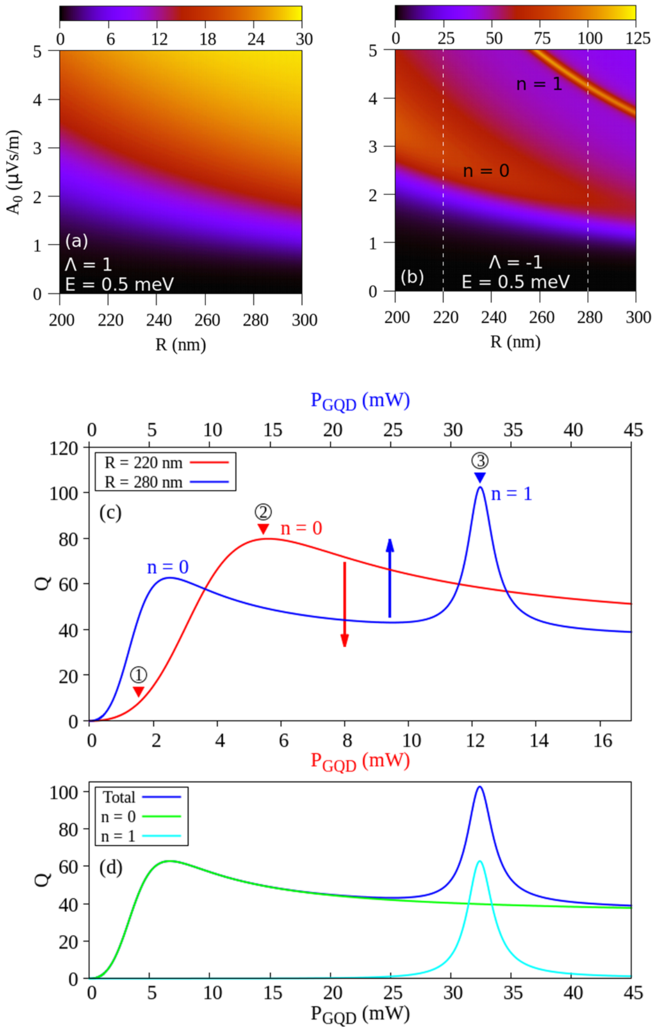

FIG. 5. Scattering efficiency as a function of R and A_0 (P_{GQD}) for the scattering modes $n = 0$ and $n = 1$. (a) corresponds to $\Lambda = 1$ (positive helicity) and, respectively, (b) to $\Lambda = -1$ (negative helicity) for an incident electron with energy $E = 0.5$ meV. (c) shows the scattering efficiency as a function of P_{GQD} for $R = 220$ nm (red curve) and, respectively, $R = 280$ nm (blue curve) for the case of $\Lambda = -1$, as it is indicated by the white dashed vertical lines in (b). The values of P_{GQD} are to be read on lower (upper) horizontal axis for red (blue) curve, as it is hinted by the red (blue) vertical arrow. The most interesting pattern is observed for the case of negative helicity where the scattering efficiency reveals resonances for specific sets of R and A_0 (P_{GQD}).

mode, resonantly excited. The scattering mode $n = 0$ peak is shifted towards a lower power of the TL and the maximum value of the scattering efficiency diminishes. On the other hand, the $n = 1$ scattering mode resonance is centered on a higher TL power $P_{\text{GQD}} = 32.36$ mW (see label "3"). It has a typical Lorentz profile, which indicates the absence of Fano resonances, and a very small width. For the sake of a clear description, we present in panel (d) the scattering efficiency curve for $R = 280$ nm and its corresponding components associated with scattering modes $n = 0$ (green curve) and 1 (cyan curve). We anticipate now that the narrower and nonperturbed from its specific Lorentz shape is the profile of the scattering efficiency curve, the more prominent are the trapping effects. Therefore we expect to figure out in what follows enhanced effects for $R = 280$ nm compared to $R = 220$ nm case.

Analyzing Fig. 5, we conclude that the scattering of an electron on a GQD is resonantly excited in the presence of a negative helicity TL driving. Otherwise, the positive helicity TL excites scattering phenomena as well, but the scattering is nonresonant. Taking into account this observation, in what follows, we perform an investigation dedicated only to $\Lambda = -1$ case.

We continue our discussion in terms of a real space inquiry. Now we concentrate our attention to a near field analysis, picturing the probability density and current around the GQD. This method of investigation helps in a very intuitive manner to describe and explain the scattering process. Each column of panels in Fig. 6 is dedicated to one of the three scattering regimes indicated by labels "1," "2," and "3" in Fig. 5(c).

The first analyzed case is addressed to $R = 220$ nm and $P_{\text{GQD}} = 1.53$ mW [see label "1" in Fig. 5(c)]. In this scattering regime the density has slightly higher values in the inner region of the dot [see Fig. 6(a)]. The spatial localization of the dot is indicated with white circle. It is well known that a permanent trapping of an electron (at normal incidence) inside a GQD is suppressed by Klein tunneling, but nevertheless, it was reported in a number of papers that there may exist some so called *quasibound states* which describe the transitory trapping of electrons for a finite period of time [49,50,52,53]. In this case, we say that the electron is *quasilocalized*. Generally speaking, the quasibound states in a GQD arise due to the generation of density current vortices inside the dot, which trap the electron for a finite period of time and after that, the electron escapes in the outer region of the dot. Indeed, analyzing Fig. 6(b), we observe at the top and, respectively, bottom edges of the GQD how the current tends to follow a vortexlike trajectory. The spatial extension of the dot is represented with blue circle. Nevertheless, since the power of the TL is not high enough, the current does not describe a closed path. The only noticeable effect takes place close to the boundary of the dot, where the quasilocalization is obviously very weak. This behavior could be anticipated, taking into account that at this TL power the scattering efficiency has a very low value [see Fig. 5(c)]. As well, we notice that the backscattering is absent and an important amount of current is directed forward, as a signature of Klein tunneling.

The second investigated scattering regime is for $R = 220$ nm and $P_{\text{GQD}} = 4.95$ mW [see label "2" in Fig. 5(c)]. Recall that these parameters correspond to the scattering resonance peak due to the excitation of $n = 0$ mode. Also in this case, the density pattern presents the highest values near the inner boundary of the GQD, but the values are about four times higher than in the previous case [see Fig. 6(c)]. The density does not display a very different behavior, but otherwise the near field current flow is more interesting, as can be seen in panel (d). In this case, the Klein tunneling still manifests, but newly, two completely closed counter-rotating vortices which trap the electron may be observed inside the dot and this is the reason for the increasing of the density values. In this regime, the backscattering is also absent, but the Klein tunneling is depleted because there exist two regions

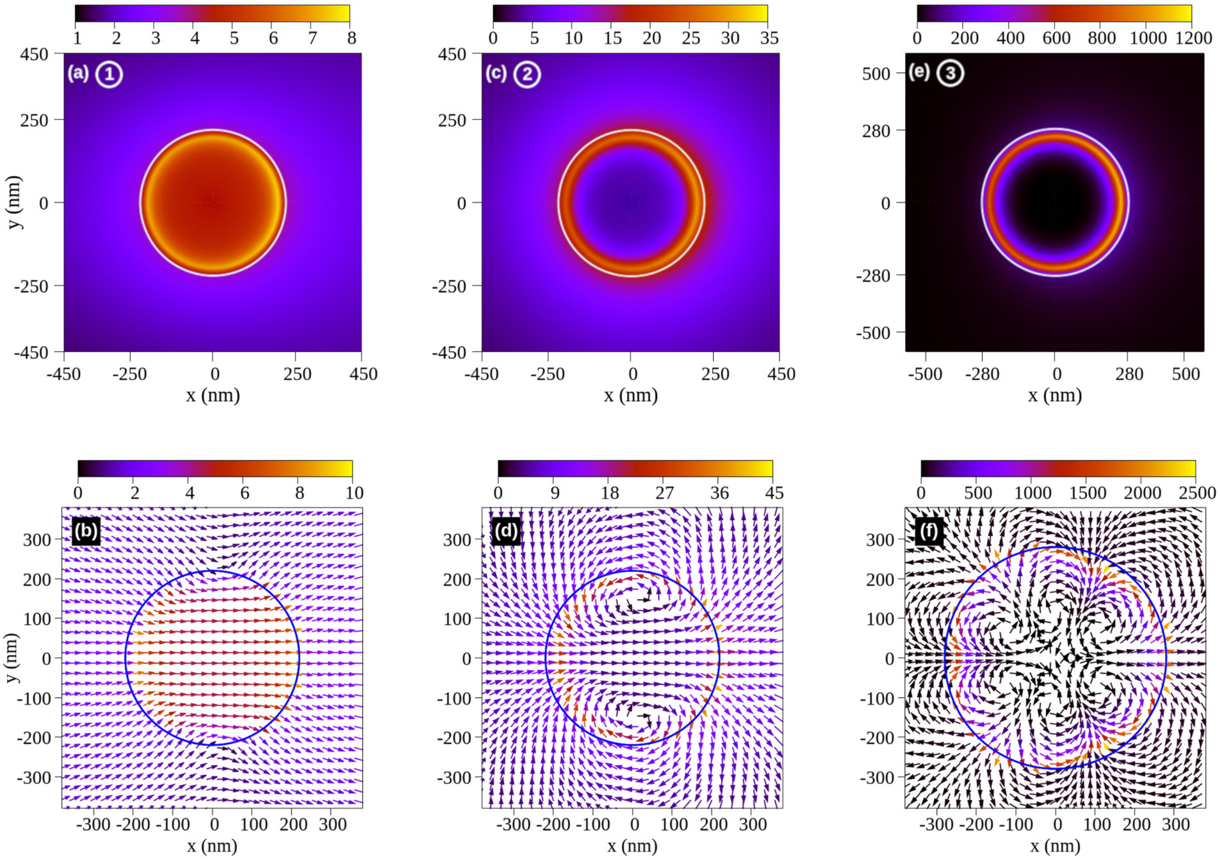

FIG. 6. Real space scattering analysis of an electron on a TL driven GQD. In each column the first panel presents the near field probability density ρ plotted as a function of coordinates and in the second panel is figured the flow in the near field of the probability current density $\mathbf{j}$: [(a) and (b)] $R = 220$ nm and PGQD $= 1.53$ mW, [(c) and (d)] $R = 220$ nm and PGQD $= 4.95$ mW, and [(e) and (f)] $R = 280$ nm and $P_{\text{GQD}} = 32.36$ mW. Each column of panels is dedicated to one scattering regime from those indicated by labels "1," "2," and "3" in Fig. 5(c). The GQD spatial localization is indicated with a white circle in the density panels and, respectively, with blue circles in the current panels. (a) The density has slightly higher values in the inner region of the dot. (b) The current tends to follow a vortexlike trajectory. (c) The density begins to exhibit higher values inside the dot. (d) Two completely closed counter-rotating vortices may be observed inside the dot. (e) The density pattern shows the higher values inside the dot. (f) Six counter-rotating vortices are generated inside the GQD.

where the impact of the electron takes place at nonnormal angles.

The third scattering analysis is performed for $R = 280$ nm and $P_{\text{GQD}} = 32.36$ mW [see label "3" in Fig. 5(c)]. This parameters correspond to the peak of the scattering resonance associated to the excitation of the $n = 1$ mode. As in the previous two cases, the density maximum is reached again close to the inner boundary of the dot [see Fig. 6(e)], which seems to be a behavior specific to such a system. Even though, in conformity with the shape and width of the scattering efficiency curve [see Fig. 5, panels (c) and (d)], as we already anticipated, the values of the density are up to two orders of magnitude as high compared to the first case and about four times higher than in the previous case. As in the second analyzed situation, the rising of the density values may be understood in terms of current. Assessing the current flow [Fig. 6(f)], we can observe this time six counter-rotating vortices which are generated inside the GQD up to the center of the dot unlike the previous case where the vortices were generated only on the extremities. Also in the present regime, the quasilocalization of the incident electron may be explained as a suppression of the Klein tunneling, since this time there arise six distinct regions where the electron penetrates the dot from outside.

So far we argued that the negative helicity TL driving may help to reach quasibound states for appropriate choices of the GQD radius and TL power. As well, we have described the trapping effects in a very intuitive manner showing the density patterns and explained the phenomenon in terms of current. In what follows, for a more comprehensive analysis, we perform an evaluation concerning the lifetime of the quasibound states in those scattering regimes where they occur. This time we treat the case of unbiased configuration. Let us shortly discuss the method.

As we have already seen, the quasibound states, not being real bound states, are characterized by positive valued energies in the continuum. The hint is to not restrict ourselves only to real values but analyze the resonances in terms of complex valued energies $E = E_r - iE_i$, where E_r is the resonant energy and E_i is the part related to the lifetime (τ) of the quasibound state by $\tau = \hbar/E_i$. In order to determine these energies, we match the transmitted wave inside the dot with the reflected wave, on the boundary of the GQD, by virtue of continuity [49]. Considering this boundary condition, we deal with the

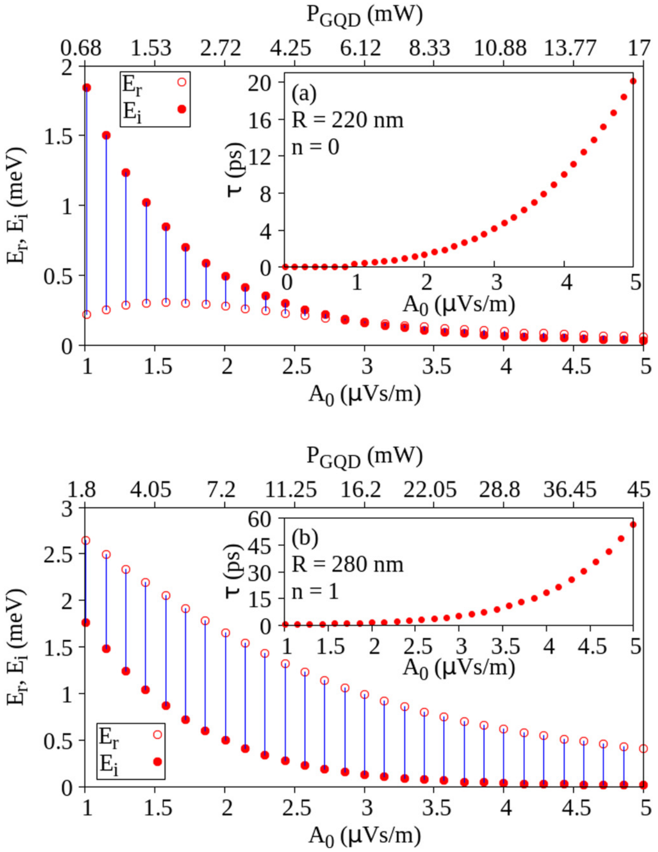

FIG. 7. Real (empty dots) and, respectively, imaginary (filled dots) parts of the complex energy $E = E_r - iE_i$ corresponding to each resonance identified at given values of A_0 (P_{GQD}) for (a) $R =$ 220 nm, $n = 0$ and (b) $R = 280$ nm, $n = 1$. The trapping time is presented in the inset.

following transcendental equation for $k = \kappa$:

$$\frac{\phi_\kappa^A}{\phi_\kappa^B} = \left.\frac{H_n(kr)}{H_{n+1}(kr)}\right|_{r=R}, \tag{50}$$

for a given mode $n = 0, 1, 2,...$ In our approach, we consider complex valued wave number $k = k_r - ik_i$ and the lifetime of the quasibound state characterized by resonant energy $E_r = v_F \hbar k_r$ is given by $\tau = 1/v_F k_i$. Each solution of Eq. (50) represents a scattering resonance in the energy space.

We solved numerically Eq. (50) and for each found resonance we present in Fig. 7 sets of values (E_r, E_i) with open and, respectively, filled dots for different values of A_0 (P_{GQD}). The radii of the dots were chosen the same as in the previous analysis, respectively $R = 220$ nm and $R = 280$ nm. The two values in each set are connected by blue lines in order to qualitatively evaluate the lifetime of the quasibound state for its corresponding resonant E_r at every given A_0 (P_{GQD}). In the inset of each panel is presented the lifetime of the quasibound states.

In Fig. 7(a), we analyze the case for $R = 220$ nm and $n = 0$. From the very beginning we observe that the increasing TL power strongly influences the lifetime of the quasibound states, reaching values of 20 ns. Even though in this case we observe the smallest trapping times with respect to the other case [see panel (b)], compared to the results presented in Refs. [27,49] ($\tau \sim 10^{-5}$ ns, respectively, $\tau \sim 10^{-4}$ ns), in our case, the lifetime is higher with two orders of magnitude, which is an outstanding trapping feature of a GQD. For the $n = 1$ scattering mode [Fig. 7(b)], the trapping times are a little bit higher, but of the same order of magnitude.

As well, we can observe performing this investigation that the trapping effects are excited at different resonant energies, depending on the scattering mode. For the case of $n = 0$, the resonant energy ranges above 0.06 up to 0.3 meV, while for $n = 1$, the energy lies in a slightly wider range, from 0.4 to 2.6 meV. Nevertheless, the energy of the incident electron must be carefully chosen, since as we can see in Fig. 7 analyzing the imaginary parts of the energy, the noticeable effects are generated for the low values of resonant energy, for both scattering modes. Having in mind this finding, we infer that, besides the radius of the dot and TL power, the energy of the incident electron plays a crucial role in the controlling of the trapping characteristics of GQDs.

IV. SUMMARY AND CONCLUSIONS

All the striking trapping effects, in the case of frequency $\omega = 10^{14}$ s^{-1}, topological charge $m = 1$ and opening angle $\theta_k = 30^\circ$ for an incident electron with energy $E = 0.5$ meV, were observed for negative helicity ($\Lambda = -1$), in which case the spin and orbital angular momentum of the TL are oriented in opposite directions. In this configuration, the scattering effects are governed by resonant excitations of $n = 0$ and $n = 1$ modes, depending on the radius of the dot and, the most interesting, the power of the driving TL.

Analyzing the scattering phenomenon in terms of probability density and current, we noticed particularities for each excited scattering mode and for each scattering regime. In the case of a resonant regime, there arise trapping processes, more prominent for $n = 1$ mode than for $n = 0$, as predicted also by analyzing the scattering efficiency curve. The quasilocalization of the incident electron revealed by density patterns, may be understood in terms of current. For $n = 0$ mode, we observed two counter-rotating vortices which induce the quasibound states and for $n = 1$, six such vortices. Moreover, the quasilocalization may be explained as a reduction of Klein tunneling which, however, is always present. For all the studied cases, the backscattering is completely suppressed and the Klein tunneling is present.

Regarding the trapping time, we proved that the higher is the power of the driving TL, the longer lasts the corresponding quasibound state, for the case of unbiased dot. We observed important values, much higher than those reported for instance in the case of electrostatic defined GQDs.

In conclusion, if the trapping of incident electrons at normal angles on GQDs seems to be impossible or the calculated/measured trapping times was reported to be very reduced, in the case of a TL driven GQD, we have proven here that, for a suitable chosen sets of parameters, the trapping can be achieved with long lasting periods of time.

The method we chose in order to analyze the scattering process of electrons on TL driven GQDs, in the case of Dirac cones approximation, seemed to be quite elegant and easy to apply, from the mathematical point of view, but with the price of imposing specific limitations regarding the parameters which govern the process. Nevertheless, our approach enabled us to reveal remarkable behaviors of the studied system, in principal, from the fundamental physical point of view. Moreover, all the effects we noticed here may be identified with possible future developments of graphene-based electronic devices.

APPENDIX: AVERAGED TOTAL POWER OF TL

In this Appendix, we briefly present the derivation of the averaged total power P_{GQD} of the TL which irradiates the GQD. We have introduced the subscript "GQD" in order to highlight that we compute the integration with respect to the GQD geometry and, as we will show, the final values depend on the radius of the GQD.

We start from the Poynting vector

$$\mathbf{S}(r,\varphi,t)=\frac{1}{\mu_0}\mathbf{E}(r,\varphi,t)\times\mathbf{B}(r,\varphi,t). \tag{A1}$$

The vector $\mathbf{S}(r,\varphi,t)$ represents a measure of the electromagnetic energy flow through a normal unit area per unit time. In Eq. (A1), the constant factor $\mu_0=4\pi\times10^{-7}$ H/m is the vacuum permeability and

$$\mathbf{E}(r,\varphi,t)=\Re[-\partial_t\mathbf{A}(r,\varphi,t)] \text{ and } \mathbf{B}(r,\varphi,t)=\Re[\nabla \times\mathbf{A}(r,\varphi,t)] \tag{A2}$$

are the electric and, respectively, magnetic fields with $\mathbf{A}(r,\varphi,t)$ being the vector potential.

The total energy per unit time which flows through the surface of the circular GQD is defined as the flux of the Poynting vector

$$P_{\mathrm{GQD}}^{\mathrm{tot}}(t)=\oint_{\mathrm{GQD}}\mathbf{S}(r,\varphi,t)\cdot\mathbf{n}ds=\int_0^R\int_0^{2\pi}S_z(r,\varphi,t)rdrd\varphi. \tag{A3}$$

We define the averaged total power TL as the averaged Poynting vector flux over a period of oscillation:

$$P_{\mathrm{GQD}}=\frac{1}{2\pi/\omega}\int_0^{2\pi/\omega}P_{\mathrm{GQD}}^{\mathrm{tot}}(t)dt. \tag{A4}$$

Using the vector potential (4), particularized to our specific case of topological charge $m=1$ and $\Lambda=-1$, we obtain from Eqs. (A2) the following components of the electric and, respectively, magnetic field:

$$E_r(r,\varphi,t)=-A_0\omega J_1(qr)\sin(k_zz-\omega t); \tag{A5}$$

$$E_\varphi(r,\varphi,t)=A_0\omega J_1(qr)\cos(k_zz-\omega t); \tag{A6}$$

$$E_z(r,\varphi,t)=-A_0\omega\tan\theta_kJ_0(qr)\cos(k_zz-t\omega); \tag{A7}$$

$$B_r(r,\varphi,t)=-A_0q\cot\theta_kJ_1(qr)\cos(k_zz-\omega t); \tag{A8}$$

$$B_\varphi(r,\varphi,t)=-A_0q(\tan\theta_k+\cot\theta_k)J_1(qr)\sin(k_zz-\omega t); \tag{A9}$$

$$B_z(r,\varphi,t)=A_0qJ_0(qr)\sin(k_zz-\omega t). \tag{A10}$$

In order to derive Eqs. (A5) and (A10), we have took into account the following transformations of the unit vectors from rectangular to cylindrical coordinates:

$$\hat{\mathbf{x}}=\cos\varphi\hat{\boldsymbol{r}}-\sin\varphi\hat{\boldsymbol{\varphi}}, \tag{A11}$$

$$\hat{\mathbf{y}}=\sin\varphi\hat{\boldsymbol{r}}+\cos\varphi\hat{\boldsymbol{\varphi}}, \tag{A12}$$

$$\hat{\mathbf{z}}=\hat{\mathbf{z}}. \tag{A13}$$

If we insert Eqs. (A5) and (A10) in Eq. (A1), we compute the following expression for the z component of the Poynting vector:

$$S_z(r,\varphi,t)=\frac{A_0^2\omega q}{\mu_0}\left[\cot\theta_k+\frac{\tan\theta_k}{2}[1-\cos(2k_zz-2\omega t)]\right]\times J_1^2(qr). \tag{A14}$$

We note that for $\Lambda=+1$, even though the expressions of the electric and magnetic field components are different, the same result for S_z still holds.

Inserting Eq. (A14) into Eq. (A3) and taking into account Eq. (A4), we find the following relation:

$$P_{\mathrm{GQD}}=\beta A_0^2, \tag{A15}$$

were β is defined as

$$\beta=\frac{\omega}{\mu_0R}\left(\cot\theta_k+\frac{\tan\theta_k}{2}\right)\times\left[qRJ_0^2(qR)-2J_0(qR)J_1(qR)+qRJ_1^2(qR)\right]. \tag{A16}$$

Using SI conventional units $[P_{\mathrm{GQD}}]$=1 W and $[A_0]$ =1 V s m^{-1}, in our case, for $\omega=10^{14}$ s^{-1} and $\theta_k=30^\circ$, it is convenient to introduce the following relation between P_{GQD} and A_0:

$$P_{\mathrm{GQD}}(\mathrm{W})=\beta A_0^2(\mu\mathrm{V\,s\,m^{-1}}); \tag{A17}$$

$$\beta=0.68 \quad \text{for} \quad R=220\text{ nm}; \tag{A18}$$

$$\beta=1.8 \quad \text{for} \quad R=280\text{ nm}. \tag{A19}$$

[1] S. V. Syzranov, Ya. I. Rodionov, K. I. Kugel, and F. Nori, Phys. Rev. B **88**, 241112(R) (2013).

[2] H. L. Calvo, H. M. Pastawski, S. Roche, and L. E. F. Foa Torres, Appl. Phys. Lett. **98**, 232103 (2011).

[3] O. V. Kibis, K. Dini, I. V. Iorsh, and I. A. Shelykh, Phys. Rev. B **95**, 125401 (2017).

[4] F. J. López-Rodríguez and G. G. Naumis, Phys. Rev. B **78**, 201406(R) (2008).

[5] J. Rioux, G. Burkard, and J. E. Sipe, Phys. Rev. B **83**, 195406 (2011).

[6] S. E. Savel'ev and A. S. Alexandrov, Phys. Rev. B **84**, 035428 (2011).

[7] O. V. Kibis, Phys. Rev. B **81**, 165433 (2010).

[8] N. M. R. Peres, A. H. Castro Neto, and F. Guinea, Phys. Rev. B **73**, 241403(R) (2006).

[9] S. Schnez, K. Ensslin, M. Sigrist, and T. Ihn, Phys. Rev. B **78**, 195427 (2008).

[10] P. Recher, J. Nilsson, G. Burkard, and B. Trauzettel, Phys. Rev. B **79**, 085407 (2009).

[11] B. Ostahie, M. Niţă, and A. Aldea, Phys. Rev. B **89**, 165412 (2014).

[12] B. Ostahie, M. Niţă, and A. Aldea, Phys. Rev. B **94**, 195431 (2016).

[13] V. Lukose, R. Shankar, and G. Baskaran, Phys. Rev. Lett. **98**, 116802 (2007).

[14] B. Ostahie, M. Niţă, and A. Aldea, Phys. Rev. B **91**, 155409 (2015).

[15] S. H. Kooi, A. Quelle, W. Beugeling, and C. M. Smith, Phys. Rev. B **98**, 115124 (2018).

[16] F. Bonaccorso, Z. Sun, T. Hasan, and A. C. Ferrari, Nat. Photon **4**, 611 (2010).

[17] G. Konstantatos, M. Badioli, L. Gaudreau, J. Osmond, M. Bernechea, F. P. G. de Arquer, F. Gatti, and F. H. L. Koppens, Nat. Nanotechnol. **7**, 363 (2012).

[18] K. M. Dani, J. Lee, R. Sharma, A. D. Mohite, C. M. Galande, P. M. Ajayan, A. M. Dattelbaum, H. Htoon, A. J. Taylor, and R. P. Prasankumar, Phys. Rev. B **86**, 125403 (2012).

[19] E. Gruber, R. A. Wilhelm, R. Pétuya, V. Smejkal, R. Kozubek, A. Hierzenberger, B. C. Bayer, I. Aldazabal, A. K. Kazansky, F. Libisch *et al.*, Nat. Commun. **7**, 13948 (2016).

[20] A. Afanasev, C. E. Carlson, and A. Mukherjee, Phys. Rev. A **88**, 033841 (2013).

[21] O. Matula, A. G. Hayrapetyan, V. G. Serbo, A. Surzhykov, and S. Fritzsche, J. Phys. B: At. Mol. Opt. Phys. **46**, 205002 (2013).

[22] H. M. Scholz-Marggraf, S. Fritzsche, V. G. Serbo, A. Afanasev, and A. Surzhykov, Phys. Rev. A **90**, 013425 (2014).

[23] M. B. Farías, G. F. Quinteiro, and P. I. Tamborenea, Eur. Phys. J. B **86**, 432 (2013).

[24] K. S. Novoselov, A. K. Geim, S. V. Morozov, D. Jiang, M. I. Katsnelson, I. V. Grigorieva, S. V. Dubonos, and A. A. Firsov, Nature (London) **438**, 197 (2005).

[25] M. I. Katsnelson, K. S. Novoselov, and A. K. Geim, Nat. Phys. **2**, 620 (2006).

[26] J. Lee, D. Wong, J. Velasco, Jr., J. F. Rodriguez-Nieva, S. Kahn, H. Z. Tsai, T. Taniguchi, K. Watanabe, A. Zettl, F. Wang *et al.*, Nat. Phys. **12**, 1032 (2016).

[27] C. Gutiérrez, L. Brown, C. J. Kim, J. Park, and A. N. Pasupathy, Nat. Phys. **12**, 1069 (2016).

[28] A. De Martino, L. Dell'Anna, and R. Egger, Phys. Rev. Lett. **98**, 066802 (2007).

[29] Y. Pan, H. Ji, X. Q. Li, and H. Liu, Sci. Rep. **10**, 20426 (2020).

[30] A. H. Castro Neto, F. Guinea, N. M. R. Peres, K. S. Novoselov, and A. K. Geim, Rev. Mod. Phys. **81**, 109 (2009).

[31] M. Loewe, F. Marquez, and R. Zamora, J. Phys. A: Math. Theor. **45**, 465303 (2012).

[32] G. F. Quinteiro, C. T. Schmiegelow, D. E. Reiter, and T. Kuhn, Phys. Rev. A **99**, 023845 (2019).

[33] J. H. Shirley, Phys. Rev. **138**, B979 (1965).

[34] U. De Giovannini and H. Hübener, J. Phys. Mater. **3**, 012001 (2020).

[35] K. Kristinsson, O. V. Kibis, S. Morina, and I. A. Shelykh, Sci. Rep. **6**, 20082 (2016).

[36] M. A. Sentef, M. Claassen, A. F. Kemper, B. Moritz, T. Oka, J. K. Freericks, and T. P. Devereaux, Nat. Commun. **6**, 7047 (2015).

[37] M. Vogl, M. Rodriguez-Vega, and G. A. Fiete, Phys. Rev. B **101**, 235411 (2020).

[38] T. Mikami, S. Kitamura, K. Yasuda, N. Tsuji, T. Oka, and H. Aoki, Phys. Rev. B **93**, 144307 (2016).

[39] N. M. R. Peres, J. N. B. Rodrigues, T. Stauber, and J. M. B. Lopes dos Santos, J. Phys.: Condens. Matter **21**, 344202 (2009).

[40] A. M. Mathai, *A Handbook of Generalized Special Functions for Statistical and Physical Sciences* (Clarendon Press, Oxford, 1993), p. 129.

[41] Y. L. Luke, *The Special Functions and Their Approximations; Mathematics in Science and Engineering* Vol. 53 (Academic Press: New York, USA; London, 1969), Vol. I, p. 216, Eq. (41).

[42] http://functions.wolfram.com/07.34.21.0003.01

[43] http://functions.wolfram.com/07.22.21.0002.01

[44] J. Cserti, A. Pályi, and C. Péterfalvi, Phys. Rev. Lett. **99**, 246801 (2007).

[45] F. Guinea, J. Low Temp. Phys. **153**, 359 (2008).

[46] R. L. Heinisch, F. X. Bronold, and H. Fehske, Phys. Rev. B **87**, 155409 (2013).

[47] C. Schulz, R. L. Heinisch, and H. Fehske, Quant. Matt **4**, 346 (2015).

[48] H. Yang, Nat. Phys. **12**, 994 (2016).

[49] P. Hewageegana and V. Apalkov, Phys. Rev. B **77**, 245426 (2008).

[50] H.-Y. Chen, V. Apalkov, and T. Chakraborty, Phys. Rev. Lett. **98**, 186803 (2007).

[51] A. E. Miroshnichenko, S. Flach, and Y. S. Kivshar, Rev. Mod. Phys. **82**, 2257 (2010).

[52] N. Freitag, L. A. Chizhova, P. Nemes-Incze, C. R. Woods, R. V. Gorbachev, Y. Cao, A. K. Geim, K. S. Novoselov, J. Burgdörfer, F. Libisch *et al.*, Nano Lett. **16**, 5798 (2016).

[53] Z.-Q. Fu, K.-K. Bai, Y.-N. Ren, J.-J. Zhou, and L. He, Phys. Rev. B **101**, 235310 (2020).